

Cell-Free MIMO with Rotatable Antennas: When Macro-Diversity Meets Antenna Directivity

Xingxiang Peng, Qingqing Wu, Ziyuan Zheng, Yanze Zhu, Wen Chen, Penghui Huang,
Ying Gao, and Honghao Wang

Abstract—Cell-free networks leverage distributed access points (APs) to achieve macro-diversity, yet their performance is often constrained by large disparities in channel quality arising from user geometry and blockages. To address this, rotatable antennas (RAs) add a lightweight hardware degree of freedom by steering the antenna boresight toward dominant propagation directions to strengthen unfavorable links, thereby enabling the network to better exploit macro-diversity for higher and more uniform performance. This paper investigates an RA-enabled cell-free downlink network and formulates a max-min rate problem that jointly optimizes transmit beamforming and antenna orientations. To tackle this challenging problem, we develop an alternating-optimization-based algorithm that iteratively updates the beamformers via a second-order cone program (SOCP) and optimizes the antenna orientations using successive convex approximation. To reduce complexity, we further propose an efficient two-stage scheme that first designs orientations by maximizing a proportional-fair log-utility using manifold-aware Frank-Wolfe updates, and then computes the beamformers using an SOCP-based design. Simulation results demonstrate that the proposed orientation-aware designs achieve a substantially higher worst-user rate than conventional beamforming-only benchmarks. Furthermore, larger antenna directivity enhances fairness with proper orientation but can degrade the worst-user performance otherwise.

Index Terms—Antenna orientation optimization, cell-free, max-min fairness, rotatable antennas.

I. INTRODUCTION

THE sixth-generation (6G) wireless network is expected to evolve toward greener, more flexible, and lightweight architectures while supporting ultra-high data rates, massive connectivity, and a uniformly high quality of experience [1]. Achieving these targets requires reliable and spatially uniform service despite uneven link qualities, co-channel interference, and dynamic traffic loads. However, conventional cell-centric designs suffer from boundary effects and inter-cell disparities, making it challenging to guarantee consistent performance for cell-edge and disadvantaged users [2]–[4].

To address these limitations, cell-free massive multiple-input multiple-output (MIMO) has emerged as a promising network architecture for beyond-5G and 6G systems [5], [6]. In a cell-free network, a large number of geographically distributed, low-complexity access points (APs) are connected to one or more central processing units (CPUs) via fronthaul

links and cooperate to serve users in a non-cellular manner, thereby removing fixed cell boundaries. By allowing each user to benefit from multiple nearby APs, cell-free transmission provides macro-diversity and effectively mitigates cell-edge degradation, leading to more uniform service quality over the coverage area. Moreover, the reduced access distances and distributed cooperation can enhance spectral and energy efficiency, while offering greater flexibility in deployment and load balancing compared to conventional cellular architectures [7]–[9]. Building on these architectural advantages, extensive research has investigated how to better harness cell-free cooperation through joint signal processing and resource optimization. In particular, coordinated beamforming and power control across distributed APs can markedly improve interference management, thereby reducing the transmit power required to meet a given quality-of-service target [10], [11]. Additional works have explored a range of performance objectives, including energy-efficiency optimization [12], spectral-efficiency maximization [13], and fairness-oriented formulations that aim to provide more consistent service quality across users [14].

Beyond beamforming and power control, there is growing interest in further enhancing cell-free performance with limited additional hardware and energy overhead, toward greener and lightweight 6G deployments. This has spurred the incorporation of reconfigurable physical-layer technologies into the cell-free architecture, with representative examples including intelligent reflecting surfaces (IRSs) and movable antennas (MAs) [15]–[17]. An IRS is a nearly passive metasurface that applies programmable phase shifts to the incident waveform, enabling low-cost control of the effective propagation environment [18]–[20]. In IRS-aided cell-free networks, the resulting reflected paths can strengthen weak or blocked AP–user links and facilitate more effective multi-AP cooperation, thereby complementing downlink beamforming in interference-limited regimes [21]–[23]. Another representative technology is the MA architecture, where antenna elements are mounted on position-adjustable platforms and can be relocated within a prescribed region to adapt the array geometry to the surrounding propagation conditions [24], [25]. Unlike IRSs that reshape the incident fields through passive reflection, MAs directly modify the transmitter/receiver geometry and hence the effective channels by changing path lengths, phases, and spatial correlation, offering a more direct and flexible means to improve channel strength and orthogonality. In cell-free networks, such geometry adaptation can alleviate the imbalance of AP–user links and enhance channel separability across users, improving the efficiency of multi-AP cooperation and

(Corresponding author: Qingqing Wu.)

The authors are with the Department of Electronic Engineering, Shanghai Jiao Tong University, 200240, China (e-mail: peng_xingxiang@sjtu.edu.cn; qingqingwu@sjtu.edu.cn; zhengziyuan2024@sjtu.edu.cn; yanzezhu@sjtu.edu.cn; wenchen@sjtu.edu.cn; huangpenghui@sjtu.edu.cn; yinggao@sjtu.edu.cn; hhwang@sjtu.edu.cn).

reducing the reliance on dense deployments [26]–[28].

However, existing studies on MA-aided cell-free systems typically assume isotropic element patterns, whereas practical AP arrays often employ directional elements. How to leverage antenna directivity to further enhance cooperation and improve service uniformity remains underexplored. The recently proposed six-dimensional movable antenna (6DMA) concept generalizes MAs by allowing joint adaptation of antenna positions and orientations [29], [30], introducing additional degrees of freedom for link alignment and interference mitigation [31]–[34]. As a lightweight and implementation-friendly special case, rotatable antennas (RAs) or rotatable surfaces optimize the orientation dimension only [35]–[41], enabling boresight steering without physical displacement. RA-enabled designs have been explored in applications such as integrated sensing and communication [39], physical-layer security [40], and spectrum sharing [41]. Particularly, RAs are appealing for cell-free deployments with many distributed APs, where mechanical relocation and continuous position tracking can be costly, power-hungry, and slow. With directional elements, orientation control can reshape the effective channels by strengthening dominant AP–user links and suppressing interference, thereby working in concert with network-wide beamforming. Most recently, the work in [42] incorporated RAs into cell-free networks, where single-antenna APs steer their boresights and perform AP–user pairing to improve the downlink performance. Yet, moving beyond such a pairing-based design to multi-antenna APs with fully flexible multi-AP cooperation is not straightforward and remains underexplored, since boresight steering becomes tightly coupled with cooperative beamforming via orientation-dependent channel gains. This calls for a joint design to better exploit macro-diversity and unlock larger cooperation gains.

Motivated by the above discussion, this paper investigates max–min fair downlink transmission in a cell-free network, where each AP is equipped with RAs whose boresights can be steered within a prescribed angular range. Compared with conventional cell-free systems with fixed antenna orientations, RA-enabled transmission can achieve a larger macro-diversity gain by adaptively reshaping the effective AP–user links. Specifically, RA steering harnesses antenna directivity to reinforce weak AP–user links while suppressing dominant interference, thereby reducing link-quality disparity and facilitating cooperation across more AP–user links. As a result, RA can enhance distributed downlink beamforming beyond what is achievable with conventional beamforming alone, thus boosting the worst-user rate of the network. Overall, the main contributions of this work are summarized as follows:

- We formulate a max–min rate maximization problem for RA-aided cell-free downlink transmission that jointly optimizes the beamformers and antenna orientations under per-AP power budgets and spherical-cap constraints. The resulting problem is highly nonconvex due to the coupling between beamforming and orientations, the orientation-dependent radiation gains embedded in the channels, and the unit-norm constraints.
- We develop an alternating-optimization (AO) framework to tackle this nonconvex problem. With fixed RA ori-

tations, the max–min beamforming subproblem is solved optimally via bisection, where each feasibility check reduces to a second-order cone program (SOCP). With fixed beamformers, the RA orientations are updated via successive convex approximation (SCA) with a relaxation of the unit-norm constraints, followed by a normalization step that restores feasibility without degrading the achieved minimum rate. Consequently, the AO iterations produce a non-decreasing minimum rate and are guaranteed to converge.

- To reduce the computational complexity, we further propose a two-stage scheme. In Stage 1, the antenna orientations are designed by maximizing a proportional-fair log-utility of users’ aggregate channel gains, which is optimized efficiently using manifold-aware Frank–Wolfe updates on the spherical-cap feasible set. In Stage 2, the beamformers are computed once using the SOCP-based max–min design with the obtained orientations.
- Simulation results demonstrate that incorporating RA orientation optimization consistently improves the worst-user rate over beamforming-only baselines and random orientation schemes. A moderate steering range already captures most of the achievable gain, which supports practical actuator constraints. The results also reveal that antenna directivity is beneficial for fairness only when the boresights are properly optimized, while misaligned highly directional elements can degrade the worst-user performance.

The remainder of this paper is organized as follows. Section II presents the system model for RA-aided cell-free downlink transmission and formulates the max–min rate optimization problem. Section III develops an AO-based algorithm to solve the formulated nonconvex problem. Section IV proposes an efficient two-stage algorithm based on proportional-fair orientation design. Section V provides numerical results and discussions, and Section VI concludes the paper.

Notations: Bold lowercase, bold uppercase, and calligraphic letters denote vectors, matrices, and sets, respectively. \mathbb{R} and \mathbb{C} denote the sets of real and complex numbers. The operators $(\cdot)^T$, $(\cdot)^H$, and $(\cdot)^*$ denote transpose, Hermitian transpose, and complex conjugate, respectively. The Euclidean norm is denoted by $\|\cdot\|_2$, and the modulus of a complex scalar x is denoted by $|x|$. The inner product of vectors \mathbf{x} and \mathbf{y} is written as $\langle \mathbf{x}, \mathbf{y} \rangle = \mathbf{x}^H \mathbf{y}$. The real-part and imaginary-part operators are denoted by $\Re\{\cdot\}$ and $\Im\{\cdot\}$, respectively. \mathbf{I} denotes the identity matrix of appropriate size. The notation $\mathbf{A} \succeq \mathbf{0}$ means that \mathbf{A} is positive semidefinite, and $\mathbf{A} \preceq \mathbf{B}$ means that $\mathbf{B} - \mathbf{A}$ is positive semidefinite. The operator $[x]_+ \triangleq \max\{0, x\}$. The natural and base-2 logarithms are denoted by $\ln(\cdot)$ and $\log_2(\cdot)$, respectively, while e and $j \triangleq \sqrt{-1}$ denote Euler’s number and the imaginary unit. The distribution $\mathcal{CN}(0, \sigma^2)$ denotes a circularly symmetric complex Gaussian random variable with zero mean and variance σ^2 , and $\mathcal{U}[a, b]$ denotes the continuous uniform distribution over $[a, b]$. The operator $\det(\cdot)$ denotes the determinant, and $\text{SO}(3)$ denotes the special orthogonal group in three dimensions.

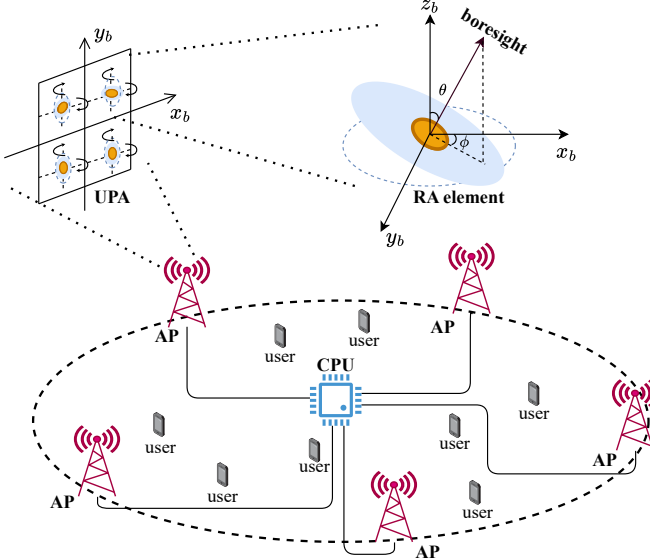


Fig. 1. A cell-free MIMO network with rotatable antennas.

II. SYSTEM MODEL AND PROBLEM FORMULATION

As shown in Fig. 1, we consider an RA-aided cell-free downlink network comprising B access points (APs) and K users. Each user is equipped with a fixed isotropic antenna, while each AP $b \in \{1, \dots, B\}$ employs a uniform planar array (UPA) of M rotatable antennas (RAs). The UPA lies in the AP's local x_b - y_b plane, where the M RAs are arranged in an $M_x \times M_y$ grid with uniform inter-element spacing d along both axes (i.e., $M = M_x M_y$). Using row-major indexing, the RA at local grid coordinate (m_x, m_y) , with $m_x \in \{1, \dots, M_x\}$ and $m_y \in \{1, \dots, M_y\}$, is assigned the index $m \in \{1, \dots, M\}$ as

$$m = m_x + (m_y - 1)M_x. \quad (1)$$

The local position of antenna element m , relative to the UPA center, is given by

$$\tilde{\mathbf{p}}_{b,m} = \begin{bmatrix} (m_x - \frac{M_x+1}{2})d \\ (m_y - \frac{M_y+1}{2})d \\ 0 \end{bmatrix}, \quad (2)$$

where the origin is at the panel's geometric center and the array normal aligns with the local z_b -axis. Let $\mathbf{R}_b \in \text{SO}(3)$ denote the rotation matrix from the local coordinate system (LCS) (x_b, y_b, z_b) to the global coordinate system (GCS), and let $\mathbf{p}_{b,0} \in \mathbb{R}^3$ denote the global coordinate of the UPA center. Then, the global position of antenna element m is given by

$$\mathbf{p}_{b,m} = \mathbf{p}_{b,0} + \mathbf{R}_b \tilde{\mathbf{p}}_{b,m}. \quad (3)$$

A. RA Model

We assume that the position and pose of each UPA remain fixed, i.e., the rotation matrix $\{\mathbf{R}_b\}_{b=1}^B$ is predetermined during deployment. However, each antenna element on the UPA can independently adjust its orientation through electronic or mechanical means. For UPA b , the orientation of element m is parameterized in its LCS by the zenith angle $\theta_{b,m}$, measured

from the local z_b -axis, and the azimuth angle $\phi_{b,m}$, measured from the local x_b -axis in the x_b - y_b plane, expressed as

$$\tilde{\mathbf{f}}_{b,m}(\theta_{b,m}, \phi_{b,m}) = \begin{bmatrix} \sin \theta_{b,m} \cos \phi_{b,m} \\ \sin \theta_{b,m} \sin \phi_{b,m} \\ \cos \theta_{b,m} \end{bmatrix}, \quad (4)$$

which inherently satisfies $\|\tilde{\mathbf{f}}_{b,m}\|_2 = 1$ by construction. To account for mechanical constraints and mitigate mutual coupling between adjacent elements, the zenith angle is constrained by

$$0 \leq \theta_{b,m} \leq \theta_{\max}, \quad \forall b, m, \quad (5)$$

where $\theta_{\max} \in [0, \frac{\pi}{2})$. This angular constraint on $\theta_{b,m}$ can be equivalently expressed as a constraint on the boresight vector:

$$\cos(\theta_{\max}) \leq \tilde{\mathbf{f}}_{b,m}^T \mathbf{e}_z \leq 1, \quad \forall b, m, \quad (6)$$

where $\mathbf{e}_z = [0, 0, 1]^T$ represents the unit vector along the z -axis in the LCS. The corresponding boresight vector in the GCS is then given by

$$\mathbf{f}_{b,m} = \mathbf{R}_b \tilde{\mathbf{f}}_{b,m}. \quad (7)$$

We model each RA element as a directional radiator. The directional gain of each RA depends on the angular offset ϵ between the signal direction and the element's main-lobe boresight, and can be modeled by a cosine pattern [41], [43]:

$$G(\epsilon) = \begin{cases} \kappa_{\max} \cos^{2p}(\epsilon), & \epsilon \in [0, \frac{\pi}{2}], \\ 0, & \text{otherwise,} \end{cases} \quad (8)$$

where $\kappa_{\max} = 2(2p+1)$ denotes the maximum gain achieved when the signal is aligned with the boresight, and p is the directivity factor controlling the main-lobe width.

B. Channel Model

We adopt a narrowband far-field model for the AP-user channels. Let $\mathbf{u}_k \in \mathbb{R}^3$ denote the global position of user k . Using the cosine-pattern gain $G(\epsilon)$ in (8) and Friis' law, the line-of-sight (LoS) link-power gain from element (b, m) to user k can be expressed as [43]

$$G_{k,b,m}^{\text{LoS}} = \beta_0 r_{k,b,m}^{-2} G(\epsilon_{k,b,m}) = \beta_0 r_{k,b,m}^{-2} \kappa_{\max} [(\mathbf{R}_b \tilde{\mathbf{f}}_{b,m})^T \mathbf{s}_{k,b,m}]_+^{2p}, \quad (9)$$

where $\beta_0 = (\lambda/4\pi)^2$, $r_{k,b,m} = \|\mathbf{p}_{b,m} - \mathbf{u}_k\|_2$, and $\mathbf{s}_{k,b,m} = \frac{\mathbf{u}_k - \mathbf{p}_{b,m}}{r_{k,b,m}}$ is the unit vector pointing from element (b, m) to user k . The corresponding LoS channel coefficient is given by

$$h_{k,b,m}^{\text{LoS}} = \sqrt{G_{k,b,m}^{\text{LoS}}} e^{-j \frac{2\pi}{\lambda} r_{k,b,m}}. \quad (10)$$

Consider Q scatterers at $\{\mathbf{c}_q\}_{q=1}^Q$ with radar cross-section (RCS) $\{\sigma_q\}_{q=1}^Q$. Define the element-scatterer distances and directions as $\tilde{r}_{q,b,m} = \|\mathbf{c}_q - \mathbf{p}_{b,m}\|_2$, and $\mathbf{s}_{q,b,m} = \frac{\mathbf{c}_q - \mathbf{p}_{b,m}}{\tilde{r}_{q,b,m}}$. Then the link-power gain from element (b, m) to scatterer q is given by

$$G_{q,b,m} = \beta_0 \tilde{r}_{q,b,m}^{-2} \kappa_{\max} [(\mathbf{R}_b \tilde{\mathbf{f}}_{b,m})^T \mathbf{s}_{q,b,m}]_+^{2p}. \quad (11)$$

Under a bistatic scattering model, the non-line-of-sight (NLoS) channel coefficient from element (b, m) to user k is given by [43]

$$h_{k,b,m}^{\text{NLoS}} = \sum_{q=1}^Q \sqrt{\frac{\sigma_q G_{q,b,m}}{4\pi \hat{r}_{k,q}^2}} e^{-j\frac{2\pi}{\lambda}(\hat{r}_{q,b,m} + \hat{r}_{k,q}) + j\chi_q}, \quad (12)$$

where $\hat{r}_{k,q} = \|\mathbf{u}_k - \mathbf{c}_q\|_2$ is the scatterer-user distance, and $\chi_q \sim \mathcal{U}[0, 2\pi)$ denotes an independent random phase. Accordingly, the total coefficient from element (b, m) to user k is given by

$$h_{k,b,m} = h_{k,b,m}^{\text{LoS}} + h_{k,b,m}^{\text{NLoS}}, \quad (13)$$

and the per-AP channel vector is expressed as

$$\mathbf{h}_{k,b} = [h_{k,b,1}, \dots, h_{k,b,M}]^T \in \mathbb{C}^M. \quad (14)$$

Remark 1 (Element-wise orientation vs. UPA pose control): In this work, we focus on element-wise RA orientation control while keeping the UPA pose matrices $\{\mathbf{R}_b\}_{b=1}^B$ fixed across the network deployment. Under this assumption, the antenna orientations affect the channel only through the directional gain terms $G(\epsilon)$ in (8), while the path lengths and associated phase shifts are governed by the static array and user/scatterer locations. Allowing the UPA poses $\{\mathbf{R}_b\}_{b=1}^B$ themselves to be reconfigurable would simultaneously change both the element positions and the array boresights, leading to joint variations in path-lengths, phases, and power patterns. Such a fully pose-adaptive architecture entails a more involved system model and is left for future work.

C. Signal Model

In the considered cell-free architecture, all APs are connected via high-capacity fronthaul links to a central processing unit (CPU). The CPU performs joint baseband processing and downlink precoding based on global channel state information (CSI). Hence, each user's data symbol can be made available at all APs to enable coherent joint transmission. The transmit signal from AP b is given by

$$\mathbf{x}_b = \sum_{k=1}^K \mathbf{w}_{k,b} s_k, \quad (15)$$

where $s_k \sim \mathcal{CN}(0, 1)$ denotes the data symbol intended for user k , and $\mathbf{w}_{k,b} \in \mathbb{C}^M$ represents the corresponding beamforming vector at AP b . The received signal at user k can then be expressed as

$$y_k = \sum_{b=1}^B \mathbf{h}_{k,b}^H \mathbf{w}_{k,b} s_k + \sum_{b=1}^B \sum_{j \neq k}^K \mathbf{h}_{k,b}^H \mathbf{w}_{j,b} s_j + n_k, \quad (16)$$

where $n_k \sim \mathcal{CN}(0, \sigma_k^2)$ denotes the additive white Gaussian noise (AWGN) at user k . For notational compactness, we stack the beamforming vectors across all APs for user k as $\mathbf{w}_k = [\mathbf{w}_{k,1}^T, \dots, \mathbf{w}_{k,B}^T]^T$, and similarly stack the corresponding channels as $\mathbf{h}_k = [\mathbf{h}_{k,1}^T, \dots, \mathbf{h}_{k,B}^T]^T$. Then the received signal at user k can be reformulated as

$$y_k = \mathbf{h}_k^H \mathbf{w}_k s_k + \sum_{j \neq k} \mathbf{h}_k^H \mathbf{w}_j s_j + n_k. \quad (17)$$

Consequently, the achievable data rate for user k is given by

$$R_k = \log_2 \left(1 + \frac{\mathbf{h}_k^H \mathbf{w}_k \mathbf{w}_k^H \mathbf{h}_k}{\mathbf{h}_k^H \sum_{j \neq k} \mathbf{w}_j \mathbf{w}_j^H \mathbf{h}_k + \sigma_k^2} \right), \quad (18)$$

where the term inside the logarithm is the signal-to-interference-plus-noise ratio (SINR) at user k .

D. Problem Formulation

We aim to jointly design the RA element orientations and downlink beamformers to maximize the minimum user rate, thereby promoting fairness among users. Since R_k in (18) is a strictly increasing function of the received SINR, this max-min rate problem is equivalently recast as a max-min SINR problem. Introducing an auxiliary variable γ to represent the worst-case user SINR, the resulting optimization problem can be written as

$$\max_{\{\tilde{\mathbf{f}}_{b,m}\}, \{\mathbf{w}_{k,b}\}, \gamma} \log_2(1 + \gamma) \quad (19)$$

$$\text{s.t.} \quad \frac{\mathbf{h}_k^H \mathbf{w}_k \mathbf{w}_k^H \mathbf{h}_k}{\mathbf{h}_k^H \left(\sum_{j \neq k} \mathbf{w}_j \mathbf{w}_j^H \right) \mathbf{h}_k + \sigma_k^2} \geq \gamma, \quad \forall k, \quad (20)$$

$$\sum_{k=1}^K \|\mathbf{w}_{k,b}\|_2^2 \leq P_{\max}, \quad \forall b, \quad (21)$$

$$\cos(\theta_{\max}) \leq \tilde{\mathbf{f}}_{b,m}^T \mathbf{e}_z \leq 1, \quad \forall b, m, \quad (22)$$

$$\|\tilde{\mathbf{f}}_{b,m}\|_2^2 = 1, \quad \forall b, m. \quad (23)$$

Here, (21) imposes a per-AP transmit power budget P_{\max} , while (22) and (23) ensure that each RA element's boresight lies on a spherical cap around the local z -axis with maximum zenith angle θ_{\max} . The above max-min design problem is difficult to solve optimally for two main reasons. First, the beamformers and orientation vectors are intricately coupled through the SINR constraints (20), leading to a highly non-convex optimization problem. Second, the spherical-cap orientation constraints (22)–(23) render the feasible set non-convex, which further complicates the design.

III. PROPOSED AO-BASED SOLUTION

This section develops an AO-based algorithm to solve the coupled max-min SINR problem. With fixed RA orientations, the beamformer subproblem is solved globally via bisection over the target SINR, where each feasibility check reduces to an SOCP. With fixed beamformers, we address the nonconvex orientation subproblem via an SCA method with a convex relaxation and a normalization step. Finally, we establish monotone convergence of the resulting AO iterations and analyze the computational complexity.

A. Optimization of Beamformers

Recall that $\mathbf{w}_k = [\mathbf{w}_{k,1}^T, \dots, \mathbf{w}_{k,B}^T]^T$ denotes the stacked beamformer for user k . With the RA orientations fixed, the

channels $\{\mathbf{h}_k\}_{k=1}^K$ are determined, and the max-min fair beamforming problem reduces to

$$\max_{\{\mathbf{w}_{k,b}\}, \gamma} \log_2(1 + \gamma) \quad (24)$$

$$\text{s.t.} \quad \frac{|\mathbf{h}_k^H \mathbf{w}_k|^2}{\sum_{j \neq k} |\mathbf{h}_k^H \mathbf{w}_j|^2 + \sigma_k^2} \geq \gamma, \quad \forall k, \quad (25)$$

$$\sum_{k=1}^K \|\mathbf{w}_{k,b}\|_2^2 \leq P_{\max}, \quad \forall b. \quad (26)$$

Exploiting the phase invariance of the SINR, we can, without loss of optimality, apply a phase rotation to \mathbf{w}_k such that $\Im\{\mathbf{h}_k^H \mathbf{w}_k\} = 0$ and $\Re\{\mathbf{h}_k^H \mathbf{w}_k\} \geq 0$. Therefore, for any target SINR $\bar{\gamma} > 0$, the constraints (25) can be equivalently written as the following second-order cone (SOC) constraints:

$$\left\| \begin{bmatrix} \mathbf{h}_k^H \mathbf{w}_1 \\ \vdots \\ \mathbf{h}_k^H \mathbf{w}_{k-1} \\ \mathbf{h}_k^H \mathbf{w}_{k+1} \\ \vdots \\ \mathbf{h}_k^H \mathbf{w}_K \\ \sigma_k \end{bmatrix} \right\|_2 \leq \frac{1}{\sqrt{\bar{\gamma}}} \Re\{\mathbf{h}_k^H \mathbf{w}_k\}. \quad (27)$$

This transformation shows that, for any fixed target SINR $\bar{\gamma}$, the beamformer design reduces to a convex SOCP feasibility problem, which can be efficiently solved using standard tools such as CVX [44]. Consequently, the globally optimal solution to the beamforming problem (24) can be obtained via a bisection search over $\bar{\gamma}$, where each iteration solves the corresponding SOCP to check feasibility.

B. Optimization of RA Orientations

With the beamformers $\{\mathbf{w}_k\}$ fixed, the RA orientation optimization problem is given by

$$\max_{\{\tilde{\mathbf{f}}_{b,m}\}, \gamma} \log_2(1 + \gamma) \quad (28)$$

$$\text{s.t.} \quad \frac{\mathbf{h}_k^H \mathbf{Q}_k \mathbf{h}_k}{\mathbf{h}_k^H \mathbf{Q}_{-k} \mathbf{h}_k + \sigma_k^2} \geq \gamma, \quad \forall k, \quad (29)$$

$$\cos(\theta_{\max}) \leq \tilde{\mathbf{f}}_{b,m}^T \mathbf{e}_z \leq 1, \quad \forall b, m, \quad (30)$$

$$\|\tilde{\mathbf{f}}_{b,m}\|_2^2 = 1, \quad \forall b, m, \quad (31)$$

where $\mathbf{Q}_k \triangleq \mathbf{w}_k \mathbf{w}_k^H$ and $\mathbf{Q}_{-k} \triangleq \sum_{j \neq k} \mathbf{w}_j \mathbf{w}_j^H$ denote the signal and interference covariance matrices, respectively. Note that, under the adopted propagation model, the effective channels $\{\mathbf{h}_k\}$ depend on the RA orientations $\{\tilde{\mathbf{f}}_{b,m}\}$. To decouple the fractional SINR constraints in (29), we introduce auxiliary variables $\{z_k > 0\}$ and obtain the following equivalent reformulation:

$$\max_{\{\tilde{\mathbf{f}}_{b,m}\}, \gamma, \{z_k\}} \log_2(1 + \gamma) \quad (32)$$

$$\text{s.t.} \quad \mathbf{h}_k^H \mathbf{Q}_k \mathbf{h}_k \geq z_k \gamma, \quad \forall k, \quad (33)$$

$$\mathbf{h}_k^H \mathbf{Q}_{-k} \mathbf{h}_k + \sigma_k^2 \leq z_k, \quad \forall k, \quad (34)$$

$$\cos(\theta_{\max}) \leq \tilde{\mathbf{f}}_{b,m}^T \mathbf{e}_z \leq 1, \quad \forall b, m, \quad (35)$$

$$\|\tilde{\mathbf{f}}_{b,m}\|_2^2 = 1, \quad \forall b, m. \quad (36)$$

The equivalence between (29) and (33)–(34) can be readily verified by contradiction. Nevertheless, the resulting problem remains highly nonconvex due to (i) the bilinear terms $z_k \gamma$ in (33), (ii) the nonconvex dependence of the signal and interference powers $\mathbf{h}_k^H \mathbf{Q}_k \mathbf{h}_k$ and $\mathbf{h}_k^H \mathbf{Q}_{-k} \mathbf{h}_k$ on the orientation variables $\tilde{\mathbf{f}}_{b,m}$, and (iii) the unit-norm constraint in (36), which renders the feasible set nonconvex. To address these issues, we adopt an SCA framework that solves a sequence of convex surrogate problems. As a first step, we upper-bound the bilinear terms $z_k \gamma$ by convex quadratic functions using Young's inequality:

$$z_k \gamma \leq \frac{1}{2} \left(\frac{z_k^{[t]}}{\gamma^{[t]}} \gamma^2 + \frac{\gamma^{[t]}}{z_k^{[t]}} z_k^2 \right), \quad \forall k, \quad (37)$$

where $\gamma^{[t]}$ and $\{z_k^{[t]}\}$ are the values obtained at the t -th SCA iteration. Substituting these upper bounds for $z_k \gamma$ in (33) yields the following intermediate surrogate problem:

$$\max_{\{\tilde{\mathbf{f}}_{b,m}\}, \gamma, \{z_k\}} \log_2(1 + \gamma) \quad (38)$$

$$\text{s.t.} \quad \mathbf{h}_k^H \mathbf{Q}_k \mathbf{h}_k \geq \frac{1}{2} \left(\frac{z_k^{[t]}}{\gamma^{[t]}} \gamma^2 + \frac{\gamma^{[t]}}{z_k^{[t]}} z_k^2 \right), \quad \forall k, \quad (39)$$

$$\mathbf{h}_k^H \mathbf{Q}_{-k} \mathbf{h}_k + \sigma_k^2 \leq z_k, \quad \forall k, \quad (40)$$

$$\cos(\theta_{\max}) \leq \tilde{\mathbf{f}}_{b,m}^T \mathbf{e}_z \leq 1, \quad \forall b, m, \quad (41)$$

$$\|\tilde{\mathbf{f}}_{b,m}\|_2^2 = 1, \quad \forall b, m. \quad (42)$$

Next, we construct quadratic surrogates for the signal and interference power functions in constraints (39) and (40)

$$\begin{cases} S_k(\{\tilde{\mathbf{f}}_{b,m}\}) \triangleq \mathbf{h}_k^H \mathbf{Q}_k \mathbf{h}_k, \\ I_k(\{\tilde{\mathbf{f}}_{b,m}\}) \triangleq \mathbf{h}_k^H \mathbf{Q}_{-k} \mathbf{h}_k. \end{cases} \quad (43)$$

The functions $S_k(\{\tilde{\mathbf{f}}_{b,m}\})$ and $I_k(\{\tilde{\mathbf{f}}_{b,m}\})$ are neither convex nor concave in $\{\tilde{\mathbf{f}}_{b,m}\}$, so a first-order Taylor expansion alone cannot yield global lower or upper bounds. To this end, we resort to the second-order Taylor expansion with suitably chosen curvature parameters.

Proposition 1 (Surrogate functions for S_k and I_k): Suppose that the antenna directivity factor satisfies $p \geq 2$. Then, for each user k , there exists a finite constant $\xi_k > 0$ such that S_k admits the following global quadratic lower bound:

$$\begin{aligned} S_k(\{\tilde{\mathbf{f}}_{b,m}\}) &\geq S_k(\{\tilde{\mathbf{f}}_{b,m}^{[t]}\}) \\ &+ \sum_{b,m} \nabla_{\tilde{\mathbf{f}}_{b,m}} S_k(\{\tilde{\mathbf{f}}_{b,m}^{[t]}\})^T (\tilde{\mathbf{f}}_{b,m} - \tilde{\mathbf{f}}_{b,m}^{[t]}) \\ &- \frac{\xi_k}{2} \sum_{b,m} \|\tilde{\mathbf{f}}_{b,m} - \tilde{\mathbf{f}}_{b,m}^{[t]}\|_2^2 \\ &\triangleq \underline{S}_k^{[t]}(\{\tilde{\mathbf{f}}_{b,m}\}), \end{aligned} \quad (44)$$

where $\{\tilde{\mathbf{f}}_{b,m}^{[t]}\}$ denotes the current SCA iterate and is treated as fixed when constructing the surrogate function. Similarly,

Algorithm 1 SCA-Based Algorithm for RA Optimization

Require: Fixed beamformers $\{\mathbf{w}_{k,b}\}$, initial orientations $\{\tilde{\mathbf{f}}_{b,m}^{[0]}\}$, tolerance $\epsilon > 0$, and maximum iterations T_{SCA}
Ensure: Optimized antenna orientations

- 1: Compute initial $\gamma^{[0]}$ and $\{z_k^{[0]}\}$;
- 2: Set $t \leftarrow 0$;
- 3: **repeat**
- 4: Construct surrogate functions $\{\underline{S}_k^{[t]}\}$ and $\{\overline{I}_k^{[t]}\}$;
- 5: Solve the convex surrogate problem (46) to obtain $\{\tilde{\mathbf{f}}_{b,m}^{[t+1]}\}$, $\gamma^{[t+1]}$, and $\{z_k^{[t+1]}\}$;
- 6: Set $t \leftarrow t + 1$;
- 7: **until** $t \geq T_{\text{SCA}}$ or $|\gamma^{[t+1]} - \gamma^{[t]}| \leq \epsilon$

there exists a finite constant $\chi_k > 0$ such that I_k admits the following global quadratic upper bound:

$$\begin{aligned} I_k(\{\tilde{\mathbf{f}}_{b,m}\}) &\leq I_k(\{\tilde{\mathbf{f}}_{b,m}^{[t]}\}) \\ &\quad + \sum_{b,m} \nabla_{\tilde{\mathbf{f}}_{b,m}} I_k(\{\tilde{\mathbf{f}}_{b,m}^{[t]}\})^T (\tilde{\mathbf{f}}_{b,m} - \tilde{\mathbf{f}}_{b,m}^{[t]}) \\ &\quad + \frac{\chi_k}{2} \sum_{b,m} \|\tilde{\mathbf{f}}_{b,m} - \tilde{\mathbf{f}}_{b,m}^{[t]}\|_2^2 \\ &\triangleq \overline{I}_k^{[t]}(\{\tilde{\mathbf{f}}_{b,m}\}). \end{aligned} \quad (45)$$

Proof: Please refer to Appendix A. \blacksquare

In the remainder of this section, we focus on the regime $p \geq 2$. Besides facilitating the surrogate construction in Proposition 1, this regime is also practically relevant. Specifically, $p \geq 2$ corresponds to moderately-to-highly directional elements, for which element-wise boresight steering can effectively exploit geometry selectivity and translate orientation control into tangible SINR/rate gains. In contrast, when $p < 2$ the power pattern becomes relatively broad and the performance is less sensitive to boresight alignment, so the benefit of element-wise orientation control is typically less pronounced. Using the bounds in Proposition 1 and relaxing the unit-norm constraints in (42) to their convex hull, we obtain the following joint convex surrogate problem at iteration t :

$$\max_{\{\tilde{\mathbf{f}}_{b,m}\}, \gamma, \{z_k\}} \log_2(1 + \gamma) \quad (46)$$

$$\text{s.t.} \quad \underline{S}_k^{[t]}(\{\tilde{\mathbf{f}}_{b,m}\}) \geq \frac{1}{2} \left(\frac{z_k^{[t]}}{\gamma^{[t]}} \gamma^2 + \frac{\gamma^{[t]}}{z_k^{[t]}} z_k^2 \right), \quad \forall k, \quad (47)$$

$$\overline{I}_k^{[t]}(\{\tilde{\mathbf{f}}_{b,m}\}) + \sigma_k^2 \leq z_k, \quad \forall k, \quad (48)$$

$$\cos(\theta_{\max}) \leq \tilde{\mathbf{f}}_{b,m}^T \mathbf{e}_z \leq 1, \quad \forall b, m, \quad (49)$$

$$\|\tilde{\mathbf{f}}_{b,m}\|_2^2 \leq 1, \quad \forall b, m. \quad (50)$$

Problem (46) can be efficiently solved by standard solvers such as CVX. Based on this surrogate, we develop an SCA-based algorithm for antenna orientation updates, as summarized in Algorithm 1. Since the convex surrogate problem (46) relaxes the unit-norm constraints (42) by their convex hull $\|\tilde{\mathbf{f}}_{b,m}\|_2^2 \leq 1$, the orientation vectors obtained from Algorithm 1 may not have unit norm. We therefore apply a normalization step to enforce the unit-norm constraints before the subsequent beamformer update.

Lemma 1 (Diagonal scaling induced by normalization): Let $\{\tilde{\mathbf{f}}_{b,m}^*\}$ be any feasible solution to problem (46) and define the normalized boresights $\tilde{\mathbf{f}}_{b,m}^{[t+1]} \triangleq \tilde{\mathbf{f}}_{b,m}^*/\|\tilde{\mathbf{f}}_{b,m}^*\|_2$, $\forall b, m$. Under the channel model (9)–(12), for every user k , the resulting stacked channel vector satisfies

$$\mathbf{h}_k\left(\{\tilde{\mathbf{f}}_{b,m}^{[t+1]}\}\right) = \mathbf{D} \mathbf{h}_k\left(\{\tilde{\mathbf{f}}_{b,m}^*\}\right), \quad (51)$$

where $\mathbf{D} \succeq \mathbf{I}$ is a diagonal matrix whose diagonal entries are $\alpha_{b,m} \triangleq \|\tilde{\mathbf{f}}_{b,m}^*\|_2^{-p}$, stacked according to the same antenna indexing order.

Proof: Since $\theta_{\max} \in [0, \frac{\pi}{2}]$, we have $\cos(\theta_{\max}) > 0$, and thus constraint (49) ensures $\|\tilde{\mathbf{f}}_{b,m}^*\|_2 \neq 0$. Fix any unit direction vector \mathbf{s} and define $\mathbf{v} \triangleq \mathbf{R}_b^T \mathbf{s}$. Then,

$$\begin{aligned} [(\mathbf{R}_b \tilde{\mathbf{f}}_{b,m}^{[t+1]})^T \mathbf{s}]_+^p &= \left[\frac{\tilde{\mathbf{f}}_{b,m}^{*T} \mathbf{v}}{\|\tilde{\mathbf{f}}_{b,m}^*\|_2} \right]_+^p = \|\tilde{\mathbf{f}}_{b,m}^*\|_2^{-p} [\tilde{\mathbf{f}}_{b,m}^{*T} \mathbf{v}]_+^p \\ &= \alpha_{b,m} [(\mathbf{R}_b \tilde{\mathbf{f}}_{b,m}^*)^T \mathbf{s}]_+^p, \end{aligned} \quad (52)$$

where $\alpha_{b,m} \triangleq \|\tilde{\mathbf{f}}_{b,m}^*\|_2^{-p}$. Moreover, by (9) and (12), $\tilde{\mathbf{f}}_{b,m}$ affects the channel only through these directional-gain factors, whereas all distance-dependent terms and the corresponding phase rotations remain unchanged. Combining this observation with (52) yields

$$h_{k,b,m}\left(\{\tilde{\mathbf{f}}_{b,m}^{[t+1]}\}\right) = \alpha_{b,m} h_{k,b,m}\left(\{\tilde{\mathbf{f}}_{b,m}^*\}\right), \quad \forall k, b, m. \quad (53)$$

Stacking over all elements gives $\mathbf{h}_k(\{\tilde{\mathbf{f}}_{b,m}^{[t+1]}\}) = \mathbf{D} \mathbf{h}_k(\{\tilde{\mathbf{f}}_{b,m}^*\})$, where \mathbf{D} is diagonal with diagonal entries $\{\alpha_{b,m}\}$. Finally, since problem (46) enforces $\|\tilde{\mathbf{f}}_{b,m}^*\|_2^2 \leq 1$, we have $\alpha_{b,m} \geq 1$ and hence $\mathbf{D} \succeq \mathbf{I}$. \blacksquare

Lemma 1 reveals that the normalization step is benign, as it does not weaken the per-element channel magnitudes and only re-weights the stacked channel by a non-attenuating diagonal scaling. This property will be used later to show that normalization preserves the monotonicity of the AO updates, and hence does not affect the convergence.

C. Overall Algorithm, Convergence, and Complexity

To sum up, Algorithm 2 summarizes the proposed AO-based design for jointly optimizing the RA orientations and the downlink beamformers. At each outer iteration, we first update the RA orientations with the beamformers fixed by invoking Algorithm 1, and then normalize the resulting orientation vectors to satisfy the unit-norm constraints. With these updated orientations fixed, we subsequently update the beamformers by solving the SOCP (24).

Proposition 2 (Monotone convergence of Algorithm 2): The minimum user rate $R_{\min}^{[t]}$ is monotonically non-decreasing with the iteration index t of Algorithm 2, and hence is guaranteed to converge.

Proof: Consider the t -th outer iteration of Algorithm 2. With fixed beamformers $\{\mathbf{w}_{k,b}^{[t]}\}$ and unit-norm orientations $\{\tilde{\mathbf{f}}_{b,m}^{[t]}\}$, the achieved worst-user SINR is $\gamma^{[t]}$. First, with $\{\mathbf{w}_{k,b}^{[t]}\}$ fixed, we update the RA orientations by solving the convex surrogate problem (46). By construction, the surrogate inequalities in problem (46) are tight at the current point

Algorithm 2 The Overall AO-Based Algorithm

Require: Initial orientations $\{\tilde{\mathbf{f}}_{b,m}^{[0]}\}$, tolerance $\epsilon_{\text{AO}} > 0$, maximum number of iterations T_{AO}

Ensure: Optimized beamformers and RA orientations

- 1: With the initial RA orientations $\{\tilde{\mathbf{f}}_{b,m}^{[0]}\}$ fixed, obtain the initial beamformers $\{\mathbf{w}_{k,b}^{[0]}\}$ by solving Problem (24);
- 2: Compute the minimum user rate $R_{\min}^{[0]}$;
- 3: Set $t \leftarrow 0$;
- 4: **repeat**
- 5: With $\{\mathbf{w}_{k,b}^{[t]}\}$ fixed, obtain a relaxed solution to RA orientations $\{\tilde{\mathbf{f}}_{b,m}^{*[t]}\}$ using Algorithm 1;
- 6: Normalize $\tilde{\mathbf{f}}_{b,m}^{[t+1]} = \tilde{\mathbf{f}}_{b,m}^{*[t]} / \|\tilde{\mathbf{f}}_{b,m}^{*[t]}\|_2, \forall b, m$;
- 7: With $\{\tilde{\mathbf{f}}_{b,m}^{[t+1]}\}$ fixed, update the beamformers $\{\mathbf{w}_{k,b}^{[t+1]}\}$ by solving Problem (24);
- 8: Compute the minimum user rate $R_{\min}^{[t+1]}$;
- 9: Set $t \leftarrow t + 1$;
- 10: **until** $t \geq T_{\text{AO}}$ or $|R_{\min}^{[t]} - R_{\min}^{[t-1]}| \leq \epsilon_{\text{AO}}$

$\{\tilde{\mathbf{f}}_{b,m}^{[t]}\}$, and $(\{\tilde{\mathbf{f}}_{b,m}^{[t]}\}, \gamma^{[t]}, \{z_k^{[t]}\})$ satisfies all the surrogate constraints. Hence, $\{\tilde{\mathbf{f}}_{b,m}^{[t]}\}$ is a feasible point of problem (46), and thus Algorithm 1 does not decrease the achievable worst-user SINR. Let γ_{sca} and $\{\tilde{\mathbf{f}}_{b,m}^{*}\}$ denote, respectively, the achieved SINR value and the resulting orientation update returned by Algorithm 1. It follows that

$$\gamma_{\text{sca}} \geq \gamma^{[t]}. \quad (54)$$

We then normalize $\{\tilde{\mathbf{f}}_{b,m}^{*}\}$ to enforce the unit-norm constraints: $\tilde{\mathbf{f}}_{b,m}^{[t+1]} = \tilde{\mathbf{f}}_{b,m}^{*} / \|\tilde{\mathbf{f}}_{b,m}^{*}\|_2, \forall b, m$. By Lemma 1, we can construct a diagonal matrix $\mathbf{D} \succeq \mathbf{I}$ such that, for all k ,

$$\mathbf{h}_k(\{\tilde{\mathbf{f}}_{b,m}^{[t+1]}\}) = \mathbf{D} \mathbf{h}_k(\{\tilde{\mathbf{f}}_{b,m}^{*}\}). \quad (55)$$

Define the scaled beamformers $\bar{\mathbf{w}}_k \triangleq \mathbf{D}^{-1} \mathbf{w}_k^{[t]}$. Then, for any k and j ,

$$\begin{aligned} \mathbf{h}_k(\{\tilde{\mathbf{f}}_{b,m}^{[t+1]}\})^H \bar{\mathbf{w}}_j &= \left(\mathbf{D} \mathbf{h}_k(\{\tilde{\mathbf{f}}_{b,m}^{*}\}) \right)^H \left(\mathbf{D}^{-1} \mathbf{w}_j^{[t]} \right) \\ &= \mathbf{h}_k(\{\tilde{\mathbf{f}}_{b,m}^{*}\})^H \mathbf{w}_j^{[t]}. \end{aligned} \quad (56)$$

Hence, all desired-signal and interference terms are exactly preserved under $(\{\tilde{\mathbf{f}}_{b,m}^{[t+1]}\}, \{\bar{\mathbf{w}}_k\})$, and thus the achieved minimum user SINR remains the same as that attained by $(\{\tilde{\mathbf{f}}_{b,m}^{*}\}, \{\mathbf{w}_k^{[t]}\})$, i.e., γ_{sca} . Moreover, since $\mathbf{D}^{-1} \preceq \mathbf{I}$, the per-AP power constraints remain satisfied:

$$\sum_{k=1}^K \|\bar{\mathbf{w}}_{k,b}\|_2^2 \leq \sum_{k=1}^K \|\mathbf{w}_{k,b}^{[t]}\|_2^2 \leq P_{\max}, \quad \forall b. \quad (57)$$

Therefore, $(\{\tilde{\mathbf{f}}_{b,m}^{[t+1]}\}, \{\bar{\mathbf{w}}_k\})$ is feasible for problem (24) with the orientations fixed at $\{\tilde{\mathbf{f}}_{b,m}^{[t+1]}\}$, and achieves the SINR γ_{sca} . Solving (24) optimally with $\{\tilde{\mathbf{f}}_{b,m}^{[t+1]}\}$ then yields an objective value no smaller than γ_{sca} , i.e.,

$$\gamma^{[t+1]} \geq \gamma_{\text{sca}} \geq \gamma^{[t]}. \quad (58)$$

Consequently, $R_{\min}^{[t]} = \log_2(1 + \gamma^{[t]})$ is non-decreasing with t . Moreover, $\{R_{\min}^{[t]}\}$ is upper-bounded due to the finite transmit power. Hence, by the monotone convergence theorem, $\{R_{\min}^{[t]}\}$ is guaranteed to converge. \blacksquare

Complexity Analysis: For the orientation optimization (Step 5 in Algorithm 2), the SCA procedure performs at most T_{SCA} iterations, and each iteration solves the convex surrogate problem (46) with worst-case complexity on the order of $\mathcal{O}((3MB + K)^{3.5})$. The subsequent normalization is a simple per-element scaling and incurs only $\mathcal{O}(MB)$ operations, which is negligible compared with the cost of solving (46). For the beamformer optimization (Step 7 in Algorithm 2), a bisection search with at most T_{bis} iterations is performed, and each iteration solves an SOCP whose worst-case complexity scales as $\mathcal{O}((BMK)^{3.5})$. As a result, the overall complexity of Algorithm 2 is $\mathcal{O}(T_{\text{AO}}(T_{\text{bis}}(BMK)^{3.5} + T_{\text{SCA}}(3MB + K)^{3.5}))$, where T_{AO} is the number of AO iterations.

IV. PROPOSED LOW-COMPLEXITY SOLUTION

The AO algorithm in the previous section achieves high max-min rate performance, but it requires solving SOCP and SCA subproblems iteratively, which may result in high computational complexity. This motivates an efficient two-stage approach proposed in this section. Specifically, we first optimize the RA orientations to shape a fair radiation profile across users, and then, with the resulting geometry fixed, solve the max-min beamforming problem using the SOCP-based method in Section III-A.

We first construct a geometry-level performance metric that depends only on the RA orientations and the physical channel. For each user k , we define its aggregate channel gain as

$$\eta_k(\{\tilde{\mathbf{f}}_{b,m}\}) \triangleq \mathbf{h}_k^H \mathbf{h}_k. \quad (59)$$

Intuitively, η_k quantifies how much signal energy the RA-aided array can deliver to user k under a given orientation geometry, irrespective of the specific beamforming vectors. To embed fairness directly at the geometry level, we adopt a logarithmic utility over the aggregate gains

$$U(\{\tilde{\mathbf{f}}_{b,m}\}) \triangleq \sum_{k=1}^K \ln(\eta_k(\{\tilde{\mathbf{f}}_{b,m}\}) + \varepsilon), \quad (60)$$

where $\varepsilon > 0$ is a small regularization constant that prevents numerical issues when η_k is close to zero. This choice is in line with the well-known PF design principle: the marginal utility with respect to η_k is

$$\frac{\partial U(\{\tilde{\mathbf{f}}_{b,m}\})}{\partial \eta_k} = \frac{1}{\eta_k(\{\tilde{\mathbf{f}}_{b,m}\}) + \varepsilon}, \quad (61)$$

which assigns larger weights to users with smaller aggregate gains and smaller weights to users with already strong gains. Consequently, maximizing $U(\{\tilde{\mathbf{f}}_{b,m}\})$ tends to allocate the RA-aided radiation more evenly across users and boost the weakest channel gains, thereby promoting a balanced radiation topology without explicitly enforcing a max-min objective. This utility serves as a geometry-level proxy that promotes balanced aggregate channel gains, which empirically provides a favorable channel realization for the subsequent max-min

beamforming. Based on the utility in (60), the RA orientation design problem is formulated as

$$\max_{\{\tilde{\mathbf{f}}_{b,m}\}} U(\{\tilde{\mathbf{f}}_{b,m}\}) \quad (62)$$

$$\text{s.t. } \cos(\theta_{\max}) \leq \tilde{\mathbf{f}}_{b,m}^T \mathbf{e}_z \leq 1, \quad \forall b, m, \quad (63)$$

$$\|\tilde{\mathbf{f}}_{b,m}\|_2^2 = 1, \quad \forall b, m. \quad (64)$$

Problem (62) remains nonconvex for two reasons: (i) the utility $U(\{\tilde{\mathbf{f}}_{b,m}\})$ couples all RA elements; and (ii) all RA orientation vectors $\{\tilde{\mathbf{f}}_{b,m}\}$ share a common nonconvex spherical-cap feasible set on the unit sphere, defined as

$$\mathcal{C}_{\text{cap}} \triangleq \{\mathbf{x} \in \mathbb{R}^3 : \|\mathbf{x}\|_2 = 1, \mathbf{x}^T \mathbf{e}_z \geq \cos(\theta_{\max})\}. \quad (65)$$

In what follows, we tackle Problem (62) using a Frank-Wolfe based algorithm. At iteration t , given a feasible orientation profile $\{\tilde{\mathbf{f}}_{b,m}^{[t]} \in \mathcal{C}_{\text{cap}}\}$, we first compute the Euclidean gradient of the utility w.r.t. each RA orientation vector

$$\nabla_{\tilde{\mathbf{f}}_{b,m}} U = \sum_{k=1}^K \frac{2\Re((\mathbf{h}_k^{[t]})^H \nabla_{\tilde{\mathbf{f}}_{b,m}} \mathbf{h}_k^{[t]})}{\eta_k^{[t]} + \varepsilon}, \quad (66)$$

where the required channel derivatives $\{\nabla_{\tilde{\mathbf{f}}_{b,m}} \mathbf{h}_k^{[t]}\}$ are given in Appendix A. To respect the unit-norm constraint, we then project $\nabla_{\tilde{\mathbf{f}}_{b,m}} U$ onto the tangent space of the unit sphere at $\tilde{\mathbf{f}}_{b,m}^{[t]}$, obtaining the Riemannian gradient on the sphere

$$\mathbf{g}_{b,m}^{[t]} \triangleq \left(\mathbf{I} - \tilde{\mathbf{f}}_{b,m}^{[t]} (\tilde{\mathbf{f}}_{b,m}^{[t]})^T \right) (\nabla_{\tilde{\mathbf{f}}_{b,m}} U). \quad (67)$$

Next, for each element we select a “target” orientation on the spherical cap by maximizing the linearized utility along $\mathbf{g}_{b,m}^{[t]}$

$$\mathbf{y}_{b,m}^{[t]} \in \arg \max_{\mathbf{x} \in \mathcal{C}_{\text{cap}}} \langle \mathbf{g}_{b,m}^{[t]}, \mathbf{x} \rangle, \quad (68)$$

whose solution can be obtained in closed-form as

$$\mathbf{y}_{b,m}^{[t]} = \begin{cases} \hat{\mathbf{g}}_{b,m}^{[t]}, & z_{b,m}^{[t]} \geq c_z, \\ \sqrt{1 - c_z^2} \mathbf{v}_{b,m}^{[t]} + c_z \mathbf{e}_z, & z_{b,m}^{[t]} < c_z, \|\mathbf{v}_{b,m}^{[t]}\|_2 \neq 0, \\ \sqrt{1 - c_z^2} \mathbf{u} + c_z \mathbf{e}_z, & z_{b,m}^{[t]} < c_z, \|\mathbf{v}_{b,m}^{[t]}\|_2 = 0, \end{cases} \quad (69)$$

where $\hat{\mathbf{g}}_{b,m}^{[t]} \triangleq \mathbf{g}_{b,m}^{[t]} / \|\mathbf{g}_{b,m}^{[t]}\|_2$, $c_z \triangleq \cos(\theta_{\max})$, $z_{b,m}^{[t]} \triangleq (\hat{\mathbf{g}}_{b,m}^{[t]})^T \mathbf{e}_z$, $\mathbf{v}_{b,m}^{[t]} \triangleq (\hat{\mathbf{g}}_{b,m}^{[t]} - z_{b,m}^{[t]} \mathbf{e}_z) / \|\hat{\mathbf{g}}_{b,m}^{[t]} - z_{b,m}^{[t]} \mathbf{e}_z\|_2$, and \mathbf{u} is any unit vector orthogonal to \mathbf{e}_z . The search direction for element (b, m) is then defined as

$$\mathbf{d}_{b,m}^{[t]} \triangleq \mathbf{y}_{b,m}^{[t]} - \tilde{\mathbf{f}}_{b,m}^{[t]}, \quad (70)$$

and all orientations are updated via a retraction

$$\tilde{\mathbf{f}}_{b,m}^{[t+1]} = \frac{\tilde{\mathbf{f}}_{b,m}^{[t]} + \rho^{[t]} \mathbf{d}_{b,m}^{[t]}}{\|\tilde{\mathbf{f}}_{b,m}^{[t]} + \rho^{[t]} \mathbf{d}_{b,m}^{[t]}\|_2}, \quad (71)$$

where $\rho^{[t]} \in (0, 1]$ is a stepsize that can be selected by a standard backtracking line search to guarantee a sufficient increase of the utility $U(\{\tilde{\mathbf{f}}_{b,m}\})$ at each accepted iteration. Given the geometry-optimized orientations from Stage 1, the effective channels $\{\mathbf{h}_k\}_{k=1}^K$ are fixed. In Stage 2, we solve the max-min fair beamforming problem (24) once, using

Algorithm 3 Proposed Low-Complexity Algorithm

Require: Initial orientations $\{\tilde{\mathbf{f}}_{b,m}^{[0]}\}$, tolerance $\epsilon > 0$, maximum number of iterations T_{FW} .

Stage 1: Orientation Design

- 1: Set $t = 0$ and $U^{[0]} = U(\{\tilde{\mathbf{f}}_{b,m}^{[0]}\})$.
- 2: **repeat**
- 3: **for** each antenna element (b, m) **do**
- 4: Compute Riemannian gradient via (67).
- 5: Compute the target orientation via (69).
- 6: Compute Frank-Wolfe search direction via (70).
- 7: **end for**
- 8: Find the stepsize $\rho^{[t]}$ via Armijo backtracking.
- 9: **for** each antenna element (b, m) **do**
- 10: Update the antenna orientation $\{\tilde{\mathbf{f}}_{b,m}^{[t+1]}\}$ via (71).
- 11: **end for**
- 12: Calculate $U^{[t+1]} = U(\{\tilde{\mathbf{f}}_{b,m}^{[t+1]}\})$.
- 13: Set $t = t + 1$.
- 14: **until** $t \geq T_{\text{FW}}$ or $|U^{[t+1]} - U^{[t]}| \leq \epsilon$

Stage 2: Beamforming Design

- 15: With antenna orientations fixed, obtain the optimal beamformers by solving problem (24).

the SOCP-based bisection method described in Section III-A. Overall, the two-stage heuristic algorithm is summarized in Algorithm 3.

Compared with the AO-based algorithm in Algorithm 2, which repeatedly alternates between SOCP-based beamforming and SCA-based orientation updates, the proposed two-stage scheme substantially reduces the computational burden by decoupling the two designs and solving the expensive beamforming subproblem only once. In Stage 1, each Frank-Wolfe iteration is dominated by gradient construction. Specifically, for each user k , computing the effective channel vector and the blockwise derivatives $\{\nabla_{\tilde{\mathbf{f}}_{b,m}} \mathbf{h}_k\}$ requires aggregating contributions from all Q paths across all BM elements, which leads to an overall cost on the order of $\mathcal{O}(KBMQ)$ per FW iteration. In contrast, the closed-form FW linear oracle on the spherical cap and the subsequent retraction updates operate in \mathbb{R}^3 per element and thus contribute only lower-order complexity. In Stage 2, with the orientations fixed, the max-min beamforming problem is solved once via SOCP bisection. Each bisection step requires solving one SOCP feasibility problem, whose dominant worst-case complexity scales as $\mathcal{O}((BMK)^{3.5})$. Let T_{FW} denote the number of FW iterations used in Stage 1, and let T_{bis} denote the number of bisection steps used in Stage 2. The overall complexity of Algorithm 3 can thus be approximated as $\mathcal{O}(T_{\text{FW}} KBMQ + T_{\text{bis}} (BMK)^{3.5})$.

V. SIMULATION RESULTS AND DISCUSSIONS

As illustrated in Fig. 2, we consider a cell-free network with $B = 5$ APs uniformly deployed on a circle of radius $R_{\text{cov}} = 300$ m at a height of $h_{\text{AP}} = 30$ m. Each AP is equipped with a UPA of $M = 4$ antennas ($M_x = 2, M_y = 2$), with an inter-element spacing of $d = \lambda/2$. The UPA’s boresight at each AP points toward the network center with a downtilt of

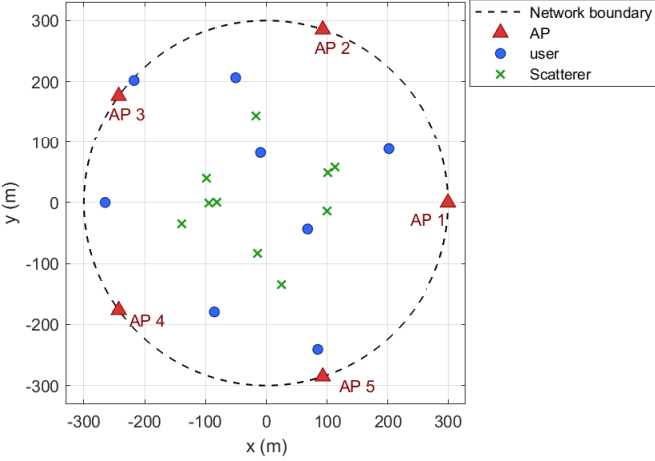


Fig. 2. Network topology. Five APs are uniformly deployed on a circle with radius $R_{\text{cov}} = 300$ m. The $K = 8$ single-antenna users are uniformly distributed within the coverage disc.

5.7°. The system serves $K = 8$ single-antenna users. All users are located at a height of $h_U = 1.5$ m, and their horizontal positions are uniformly distributed within a disc of radius R_{cov} . The carrier frequency is $f_c = 2.4$ GHz, and the noise power at each user is set as $\sigma^2 = -80$ dBm.

A. Convergence Behavior

Before the performance comparison, Fig. 3 depicts the convergence behavior of the proposed AO-based algorithm, where the transmit power budget per AP is set to $P_{\text{max}} = 15$ dBm and the antenna directivity factor is set to $p = 3$. The figure plots the minimum user rate versus the AO iteration index for three choices of the number of RA elements per AP, namely, $M \in \{2, 4, 6\}$. In all cases, the minimum rate is non-decreasing over iterations, indicating that each AO update preserves or improves the objective value. As a result, the proposed algorithm converges reliably within a modest number of iterations. Moreover, increasing M consistently improves the converged minimum rate, since a larger number of RA elements provides richer spatial degrees of freedom for both beamforming and orientation design, thereby enabling finer control of the effective channels and inter-user interference.

B. Performance Comparison

For performance comparison, we consider the following benchmark schemes:

- **Random antenna orientation:** The antenna orientations are randomly and uniformly drawn from their feasible sets to generate 30 independent configurations. For each configuration, the max-min beamforming problem is solved using the SOCP-based method, and the one achieving the largest minimum user rate is reported.
- **Isotropic antenna:** Each AP employs omnidirectional antennas (i.e., the antenna gain is orientation independent, equivalently $p = 0$ in Eq. (8)). The max-

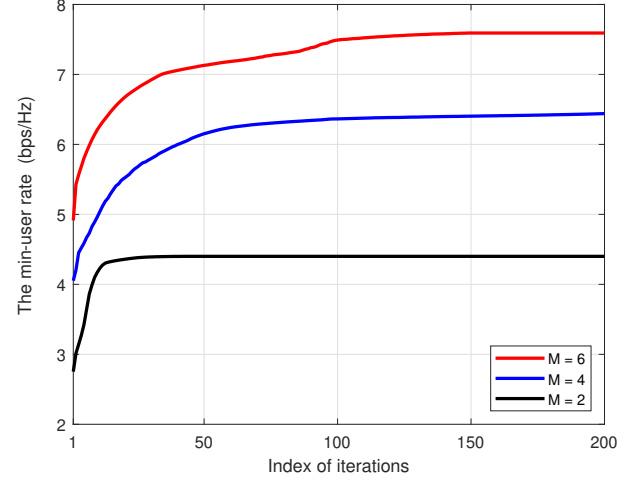


Fig. 3. The convergence behavior of the proposed AO-based algorithm.

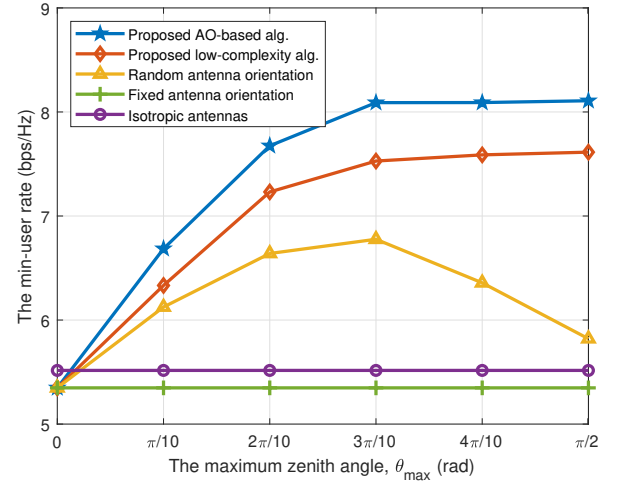


Fig. 4. The min-user rate vs. the maximum zenith angle.

min beamforming problem is then solved using the SOCP-based method.

- **Fixed antenna orientation:** The antenna orientations are fixed to their initial values without optimization. Given this fixed geometry, the max-min beamforming problem is solved using the SOCP-based method.

Fig. 4 shows the average minimum user rate versus the maximum zenith angle θ_{max} , which controls the feasible spherical-cap range of each RA orientation. We set $P_{\text{max}} = 15$ dBm and $p = 5$. As θ_{max} increases, the proposed AO-based algorithm benefits significantly from the enlarged orientation design range: its minimum rate rises rapidly from about 5.0 bps/Hz at $\theta_{\text{max}} = 0$ to ≈ 6.7 bps/Hz at $\theta_{\text{max}} = \pi/10$, and further to ≈ 7.7 bps/Hz at $\theta_{\text{max}} = 2\pi/10$. After that, the gain becomes marginal and the curve saturates around ≈ 8.1 bps/Hz when $\theta_{\text{max}} \geq 3\pi/10$, suggesting that a moderate tilt range already captures most of the RA orientation gain. The proposed low-complexity algorithm follows a similar trend but

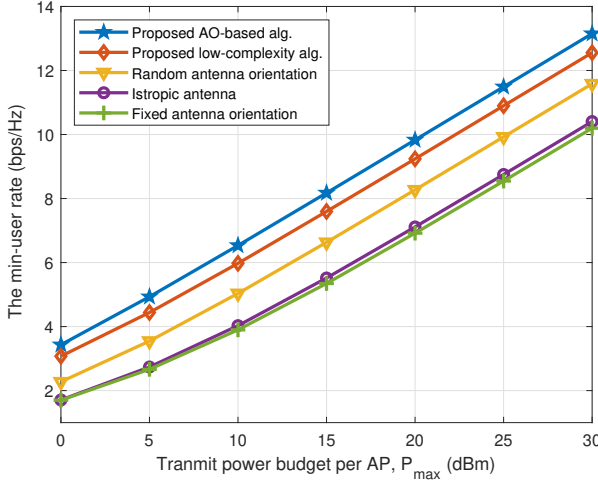


Fig. 5. The min-user rate vs. the transmit power budget per AP.

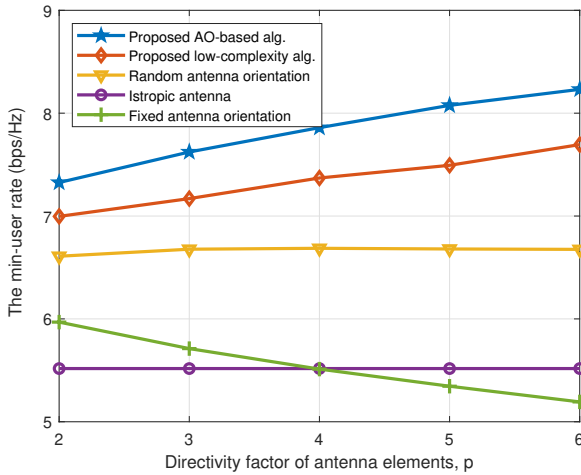


Fig. 6. The min-user rate vs. the antenna directivity factor.

converges to a lower plateau (around ≈ 7.6 bps/Hz), implying that joint AO updates can better exploit the coupling between beamforming and orientation than a decoupled design. In contrast, the “Random antenna orientation” benchmark achieves much smaller gains (peaking around 6.8 bps/Hz) and becomes unstable for large θ_{\max} , indicating that simply enlarging the feasible orientation set does not translate into fairness improvement without principled optimization. Finally, the “Isotropic antenna” and “Fixed antenna orientation” baselines remain essentially insensitive to θ_{\max} . Notably, the fixed-orientation case stays below the isotropic baseline, highlighting that strong directivity can hurt the worst-user performance unless the RA orientations are properly optimized.

Fig. 5 shows the average minimum user rate versus the transmit power budget per AP, where we set $p = 5$, and $\theta_{\max} = \pi/3$. The proposed AO-based and low-complexity algorithms consistently outperform all benchmarks over the entire power range, and their curves are nearly parallel to the

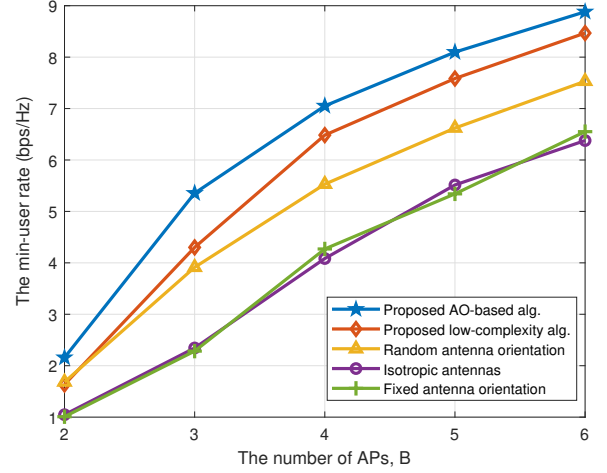


Fig. 7. The min-user rate vs. the number of APs.

baselines. For instance, at $P_{\max} = 15$ dBm, the AO-based method improves the worst-user rate by approximately 24%, 49%, and 53% over the random orientation, isotropic, and fixed orientation baselines, respectively. The low-complexity algorithm also delivers notable gains of about 15%, 38%, and 43% over the same benchmarks. These gains are attributed to RA orientation optimization, which leverages antenna directivity to reinforce weak AP–user links while suppressing dominant interference, thereby enabling more effective multi-AP cooperation and lifting the worst-user rate floor.

Fig. 6 shows the average minimum user rate versus the antenna directivity factor p , where we set $P_{\max} = 15$ dBm, and $\theta_{\max} = \pi/3$. The two proposed schemes benefit monotonically from increasing p , indicating that stronger directivity can be effectively converted into fairness gains when the RA orientations are properly adjusted and jointly designed with beamforming. In contrast, the “Fixed antenna orientation” baseline degrades noticeably as p increases, since a narrower main-lobe with misaligned boresights reduces the effective coverage of the worst users and exacerbates unfairness. The “Isotropic antenna” baseline is insensitive to p , as expected, while the “Random antenna orientation” scheme exhibits limited improvement and can even deteriorate for large p , suggesting that higher directivity is not inherently beneficial without principled orientation control. Overall, the figure highlights that directivity is a double-edged sword: it amplifies the benefits of optimized RA designs, yet can be detrimental when orientations are not properly optimized.

Fig. 7 plots the average minimum user rate versus the number of APs, where we set $P_{\max} = 15$ dBm, $p = 5$, and $\theta_{\max} = \pi/3$. As the number of APs increases, all schemes achieve higher minimum rates due to the increased spatial diversity and the enlarged set of cooperative transmit antennas, which improves the worst-user service quality. The proposed AO-based algorithm consistently attains the best performance and preserves a clear margin over the benchmarks for all B , while the proposed low-complexity design remains close but slightly inferior, reflecting the benefit of fully exploiting

the coupling between beamforming and RA orientations. The “Random antenna orientation” baseline also improves with B but stays notably below the proposed methods, indicating that cooperation alone cannot replace orientation-aware optimization under a max-min objective. Moreover, the gap between the proposed methods and the isotropic/fixed-orientation baselines becomes more pronounced as B grows, suggesting that the additional network-wide spatial degrees of freedom offered by more APs can be better leveraged when RA orientations are properly optimized.

VI. CONCLUSION

This paper studied max-min fair downlink transmission in cell-free networks enhanced by RAs. We formulated a max-min rate maximization problem that jointly optimizes the network-wide beamformers and the element-wise RA orientations under per-AP power budgets and spherical-cap steering constraints. To tackle the resulting nonconvex design, we developed an AO framework, where the beamforming subproblem is solved optimally via bisection with SOCP feasibility checks, and the orientation subproblem is handled by an SCA procedure with a relaxation of the unit-norm constraints followed by a normalization step that preserves feasibility and the achieved minimum-rate value. In addition, to reduce computational complexity, we proposed an efficient two-stage scheme that first designs the RA orientations by maximizing a proportional-fair log-utility using manifold-aware Frank-Wolfe updates, and then computes the beamformers once using the SOCP-based max-min design.

Simulation results demonstrated that incorporating RA orientation optimization consistently improves the worst-user rate over beamforming-only baselines and random orientation schemes. A moderate steering range was shown to capture most of the achievable gain, supporting practical actuation limits. The results also highlighted that antenna directivity is beneficial for fairness only when the boresights are properly optimized, whereas misaligned highly directional elements can degrade the worst-user performance. Overall, the proposed RA-aware designs provide an effective and implementation-friendly means to strengthen disadvantaged links and enhance service uniformity in cell-free deployments.

APPENDIX

A. Proof of Proposition 1

By using the chain rule, the first-order gradients of the signal and interference powers in (43) w.r.t. each element-wise boresight vector $\tilde{\mathbf{f}}_{b,m} \in \mathbb{R}^3$ are given by

$$\nabla_{\tilde{\mathbf{f}}_{b,m}} S_k = 2 \Re \left\{ w_{k,b,m}^* (\mathbf{h}_k^H \mathbf{w}_k) \nabla_{\tilde{\mathbf{f}}_{b,m}} h_{k,b,m} \right\}, \quad (74)$$

$$\nabla_{\tilde{\mathbf{f}}_{b,m}} I_k = 2 \Re \left\{ \left(\sum_{j \neq k} w_{j,b,m}^* (\mathbf{h}_k^H \mathbf{w}_j) \right) \nabla_{\tilde{\mathbf{f}}_{b,m}} h_{k,b,m} \right\}, \quad (75)$$

where $\nabla_{\tilde{\mathbf{f}}_{b,m}} h_{k,b,m}$ is given in (72) at the bottom of the page. The corresponding second-order gradients are given by

$$\begin{aligned} \nabla_{\tilde{\mathbf{f}}_{b,m}}^2 S_k = & 2 \Re \left\{ |w_{k,b,m}|^2 \nabla_{\tilde{\mathbf{f}}_{b,m}} h_{k,b,m} (\nabla_{\tilde{\mathbf{f}}_{b,m}} h_{k,b,m})^H \right\} \\ & + 2 \Re \left\{ w_{k,b,m}^* (\mathbf{h}_k^H \mathbf{w}_k) \nabla_{\tilde{\mathbf{f}}_{b,m}}^2 h_{k,b,m} \right\}. \end{aligned} \quad (76)$$

$$\begin{aligned} \nabla_{\tilde{\mathbf{f}}_{b,m}}^2 I_k = & 2 \Re \left\{ \sum_{j \neq k} |w_{j,b,m}|^2 \nabla_{\tilde{\mathbf{f}}_{b,m}} h_{k,b,m} (\nabla_{\tilde{\mathbf{f}}_{b,m}} h_{k,b,m})^H \right\} \\ & + 2 \Re \left\{ \left(\sum_{j \neq k} w_{j,b,m}^* (\mathbf{h}_k^H \mathbf{w}_j) \right) \nabla_{\tilde{\mathbf{f}}_{b,m}}^2 h_{k,b,m} \right\}. \end{aligned} \quad (77)$$

where $\nabla_{\tilde{\mathbf{f}}_{b,m}}^2 h_{k,b,m}$ is given in (73) at the bottom of the page. Due to the positive-part operator $[\cdot]_+$, when $p < 2$, the functions S_k and I_k are not second-order Lipschitz smooth in $\tilde{\mathbf{f}}_{b,m}$, so one cannot guarantee a global quadratic lower bound with a finite curvature constant. For $p \geq 2$, the quadratic lower bound in Proposition 1 can be ensured by constructing a curvature constant ξ_k such that $\|\nabla_{\tilde{\mathbf{f}}_{b,m}}^2 S_k\|_2 \leq \xi_k$ for all feasible $\tilde{\mathbf{f}}_{b,m}$ (equivalently, $\nabla_{\tilde{\mathbf{f}}_{b,m}}^2 S_k \preceq \xi_k \mathbf{I}$). Since $\|\nabla_{\tilde{\mathbf{f}}_{b,m}}^2 S_k\|_2 \leq \|\nabla_{\tilde{\mathbf{f}}_{b,m}}^2 S_k\|_F$, it suffices to upper-bound the Frobenius norm. Under the unit-norm constraint on $\tilde{\mathbf{f}}_{b,m}$, $[(\mathbf{R}_b \tilde{\mathbf{f}}_{b,m})^T \mathbf{s}]_+ \leq 1$, and the orthogonality of \mathbf{R}_b ensures that $[\cdot]_+^{p-1}$ and $[\cdot]_+^{p-2}$ are globally bounded for $p \geq 2$. Consequently, $\|\nabla_{\tilde{\mathbf{f}}_{b,m}} h_{k,b,m}\|_2$ and $\|\nabla_{\tilde{\mathbf{f}}_{b,m}}^2 h_{k,b,m}\|_F$ are bounded above. Substituting these bounds into (76) yields an explicit upper bound for $\|\nabla_{\tilde{\mathbf{f}}_{b,m}}^2 S_k\|_F$, from which a finite constant ξ_k can be constructed. Applying the same reasoning to (77) analogously provides a finite χ_k for I_k .

REFERENCES

[1] C. -X. Wang *et al.*, “On the road to 6G: Visions, requirements, key technologies, and testbeds,” *IEEE Commun. Surveys & Tut.*, vol. 25, no. 2, pp. 905-974, 2023.

$$\begin{aligned} \nabla_{\tilde{\mathbf{f}}_{b,m}} h_{k,b,m} = & \sqrt{\beta_0 \kappa_{\max}} \frac{p}{r_{k,b,m}} \left[(\mathbf{R}_b \tilde{\mathbf{f}}_{b,m})^T \mathbf{s}_{k,b,m} \right]_+^{p-1} \mathbf{R}_b^T \mathbf{s}_{k,b,m} e^{-j \frac{2\pi}{\lambda} r_{k,b,m}} \\ & + \sum_{q=1}^Q \sqrt{\beta_0 \kappa_{\max}} \sqrt{\frac{\sigma_q}{4\pi}} \frac{p}{\tilde{r}_{q,b,m} \hat{r}_{k,q}} \left[(\mathbf{R}_b \tilde{\mathbf{f}}_{b,m})^T \mathbf{s}_{q,b,m} \right]_+^{p-1} \mathbf{R}_b^T \mathbf{s}_{q,b,m} e^{-j \frac{2\pi}{\lambda} (\tilde{r}_{q,b,m} + \hat{r}_{k,q}) + j\chi_q}, \end{aligned} \quad (72)$$

$$\begin{aligned} \nabla_{\tilde{\mathbf{f}}_{b,m}}^2 h_{k,b,m} = & \sqrt{\beta_0 \kappa_{\max}} \frac{p(p-1)}{r_{k,b,m}} \left[(\mathbf{R}_b \tilde{\mathbf{f}}_{b,m})^T \mathbf{s}_{k,b,m} \right]_+^{p-2} (\mathbf{R}_b^T \mathbf{s}_{k,b,m}) (\mathbf{R}_b^T \mathbf{s}_{k,b,m})^T e^{-j \frac{2\pi}{\lambda} r_{k,b,m}} \\ & + \sum_{q=1}^Q \sqrt{\beta_0 \kappa_{\max}} \sqrt{\frac{\sigma_q}{4\pi}} \frac{p(p-1)}{\tilde{r}_{q,b,m} \hat{r}_{k,q}} \left[(\mathbf{R}_b \tilde{\mathbf{f}}_{b,m})^T \mathbf{s}_{q,b,m} \right]_+^{p-2} (\mathbf{R}_b^T \mathbf{s}_{q,b,m}) (\mathbf{R}_b^T \mathbf{s}_{q,b,m})^T e^{-j \frac{2\pi}{\lambda} (\tilde{r}_{q,b,m} + \hat{r}_{k,q}) + j\chi_q}. \end{aligned} \quad (73)$$

[2] H. Q. Ngo, G. Interdonato, E. G. Larsson, G. Caire and J. G. Andrews, "Ultradense cell-free massive MIMO for 6G: Technical overview and open questions," *Proc. IEEE*, vol. 112, no. 7, pp. 805-831, Jul. 2024.

[3] M. Mohammadi, Z. Mobini, H. Quoc Ngo and M. Matthaiou, "Next-generation multiple access with cell-free massive MIMO," *Proc. IEEE*, vol. 112, no. 9, pp. 1372-1420, Sept. 2024.

[4] E. Shi *et al.*, "RIS-aided cell-free massive MIMO systems for 6G: Fundamentals, system design, and applications," *Proc. IEEE*, vol. 112, no. 4, pp. 331-364, April 2024.

[5] H. Q. Ngo, A. Ashikhmin, H. Yang, E. G. Larsson and T. L. Marzetta, "Cell-free massive MIMO versus small cells," *IEEE Trans. Wireless Commun.*, vol. 16, no. 3, pp. 1834-1850, Mar. 2017.

[6] J. Zhang, E. Björnson, M. Matthaiou, D. W. K. Ng, H. Yang and D. J. Love, "Prospective multiple antenna technologies for beyond 5G," *IEEE J. Sel. Areas Commun.*, vol. 38, no. 8, pp. 1637-1660, Aug. 2020.

[7] E. Björnson and L. Sanguinetti, "Scalable cell-free massive MIMO systems," *IEEE Trans. Commun.*, vol. 68, no. 7, pp. 4247-4261, Jul. 2020.

[8] H. A. Ammar, R. Adve, S. Shahbazpanahi, G. Boudreau and K. V. Srinivas, "User-centric cell-free massive MIMO networks: A survey of opportunities, challenges and solutions," *IEEE Commun. Surveys & Tut.*, vol. 24, no. 1, pp. 611-652, Firstquarter 2022.

[9] S. Elhoushy, M. Ibrahim and W. Hamouda, "Cell-free massive MIMO: A survey," *IEEE Commun. Surveys & Tut.*, vol. 24, no. 1, pp. 492-523, Firstquarter 2022.

[10] N. Jayaweera, K. B. S. Manosha, N. Rajatheva and M. Latva-aho, "Minimizing energy consumption in cell-free massive MIMO networks," *IEEE Trans. Veh. Technol.*, vol. 73, no. 9, pp. 13263-13277, Sept. 2024.

[11] L. Miretti, R. Luís Garrido Cavalcante and S. Stańczak, "Two-timescale joint power control and beamforming design With applications to cell-free Massive MIMO," *IEEE Trans. Wireless Commun.*, vol. 24, no. 10, pp. 8129-8144, Oct. 2025.

[12] A. Girycki, M. A. Rahman and S. Pollin, "Energy efficiency analysis and optimization for cell-free mMIMO networks," *IEEE Trans. Mobile Computing*, Early Access, 2025, doi: 10.1109/TMC.2025.3615728.

[13] C. Feng, W. Shen, J. An and L. Hanzo, "Weighted sum rate maximization of the mmWave cell-free MIMO downlink relying on hybrid precoding," *IEEE Trans. Wireless Commun.*, vol. 21, no. 4, pp. 2547-2560, Apr. 2022.

[14] M. Farooq, H. Q. Ngo, E. -K. Hong and L. -N. Tran, "Utility maximization for large-scale cell-free massive MIMO downlink," *IEEE Trans. Commun.*, vol. 69, no. 10, pp. 7050-7062, Oct. 2021.

[15] Q. Wu *et al.*, "Integrating movable antennas and intelligent reflecting surfaces (MA-IRS): Fundamentals, practical solutions, and ISAC," arXiv preprint: 2506.14636, <http://arxiv.org/abs/2506.14636>, 2025.

[16] H. Wang *et al.*, "Reconfigurable airspace: Synergizing movable antenna and intelligent surface for low-altitude ISAC networks," arXiv preprint: 2511.10310, <http://arxiv.org/abs/2511.10310>, 2025.

[17] Y. Gao, Q. Wu, W. Mei, G. Chen, W. Chen and Z. Zheng, "Integrating movable antennas and intelligent reflecting surfaces for coverage enhancement," *IEEE Trans. Wireless Commun.*, Early Access, 2025, doi: 10.1109/TWC.2025.3623474.

[18] Q. Wu *et al.*, "Intelligent surfaces empowered wireless network: recent advances and the road to 6G," *Proc. IEEE*, vol. 112, no. 7, pp. 724-763, Jul. 2024.

[19] Q. Wu *et al.*, "Intelligent reflecting surfaces for wireless networks: Deployment architectures, key solutions, and field trials," *IEEE Wireless Commun.*, vol. 32, no. 6, pp. 141-148, Dec. 2025.

[20] Q. Wu *et al.*, "Intelligent reflecting surfaces for integrated sensing and communications: A survey," arXiv preprint: 2511.10990, <http://arxiv.org/abs/2511.10990>, 2025.

[21] Z. Sui, H. Q. Ngo, M. Matthaiou and L. Hanzo, "Performance analysis and optimization of STAR-RIS-aided cell-free massive MIMO systems relying on imperfect hardware," *IEEE Trans. Wireless Commun.*, vol. 24, no. 4, pp. 2925-2939, Apr. 2025.

[22] M. Chakraborty, E. Sharma, H. A. Suraweera and H. Quoc Ngo, "Analysis and optimization of RIS-assisted cell-free massive MIMO NOMA systems," *IEEE Trans. Commun.*, vol. 73, no. 4, pp. 2631-2647, Apr. 2025.

[23] H. Fang, H. Hu, B. Wu, Y. Zhang, L. Yang and H. Zhu, "Power allocation and precoding design for active RIS-aided cell-free massive MIMO systems," *IEEE Internet Things J.*, vol. 12, no. 9, pp. 12328-12340, May, 2025.

[24] L. Zhu *et al.*, "A tutorial on movable antennas for wireless networks," *IEEE Commun. Surveys & Tut.*, vol. 28, pp. 3002-3054, 2026.

[25] Y. Gao, Q. Wu and W. Chen, "Joint transmitter and receiver design for movable antenna enhanced Multicast communications," *IEEE Trans. Wireless Commun.*, vol. 23, no. 12, pp. 18186-18200, Dec. 2024.

[26] H. Wei, W. Wang, W. Ni, C. Zhang and Y. Huang, "Movable-antenna enabled cell-free networks," *IEEE Trans. Veh. Technol.*, vol. 74, no. 10, pp. 16533-16537, Oct. 2025.

[27] Q. Li, W. Wang, Y. Li, F. Yu, C. Zhang and Y. Huang, "Deep reinforcement learning for movable antenna-assisted cell-free networks," *IEEE Wireless Commun. Lett.*, vol. 14, no. 9, pp. 2783-2787, Sept. 2025.

[28] J. Zhu, L. Feng, X. Wang, H. Du and S. Guo, "Joint beamforming, user association, and antenna position optimization in movable antenna-assisted cell-free Massive MIMO," *IEEE Trans. Netw. Sci. Eng.*, vol. 13, pp. 4155-4171, 2026.

[29] X. Shao and R. Zhang, "6DMA enhanced wireless network with flexible antenna position and rotation: Opportunities and challenges," *IEEE Commun. Mag.*, vol. 63, no. 4, pp. 121-128, Apr. 2025.

[30] X. Shao *et al.*, "A tutorial on six-dimensional movable antenna for 6G networks: Synergizing positionable and rotatable antennas," *IEEE Commun. Surveys & Tut.*, vol. 28, pp. 3666-3709, 2026.

[31] X. Shao, R. Zhang, Q. Jiang and R. Schober, "6D movable antenna enhanced wireless network via discrete position and rotation optimization," *IEEE J. Sel. Areas Commun.*, vol. 43, no. 3, pp. 674-687, Mar. 2025.

[32] X. Pi, L. Zhu, H. Mao, Z. Xiao, X. -G. Xia and R. Zhang, "6D movable antenna enhanced multi-access point coordination via position and orientation optimization," *IEEE Trans. Wireless Commun.*, Early Access, 2025, doi: 10.1109/TWC.2025.3587803.

[33] T. Ren, X. Zhang, L. Zhu, W. Ma, X. Gao and R. Zhang, "6-D movable antenna enhanced interference mitigation for cellular-connected UAV communications," *IEEE Wireless Commun. Lett.*, vol. 14, no. 6, pp. 1618-1622, Jun. 2025.

[34] X. Shi, X. Shao, B. Zheng and R. Zhang, "6DMA-aided cell-free massive MIMO communication," *IEEE Wireless Commun. Lett.*, vol. 14, no. 5, pp. 1361-1365, May 2025.

[35] Q. Peng *et al.*, "Rotatable IRS aided wireless communication," arXiv preprint: 2511.10006, <https://arxiv.org/abs/2511.10006>, 2025.

[36] Q. Peng, Q. Wu, G. Chen, W. Chen, S. Shen, and S. Ma, "Cooperative rotatable IRSs for wireless communications: Joint beamforming and orientation optimization," arXiv preprint: 2512.14037, <https://arxiv.org/abs/2512.14037>, 2025.

[37] B. Zheng, Q. Wu, T. Ma, and R. Zhang, "Rotatable antenna enabled wireless communication: Modeling and optimization," arXiv preprint: 2501.02595, <https://arxiv.org/abs/2501.02595>, 2025.

[38] B. Zheng, T. Ma, C. You, J. Tang, R. Schober, and R. Zhang, "Rotatable antenna enabled wireless communication and sensing: Opportunities and challenges," *IEEE Wireless Commun.*, Early Access, 2025, doi: 10.1109/WMC.2025.3611919.

[39] L. Dai, B. Zheng, Q. Wu, C. You, R. Schober and R. Zhang, "Rotatable antenna-enabled secure wireless communication," *IEEE Wireless Commun. Lett.*, vol. 14, no. 11, pp. 3440-3444, Nov. 2025.

[40] C. Zhou, C. You, B. Zheng, X. Shao and R. Zhang, "Rotatable antennas for integrated sensing and communications," *IEEE Wireless Commun. Lett.*, vol. 14, no. 9, pp. 2838-2842, Sept. 2025.

[41] X. Peng, Q. Wu, Z. Zheng, W. Chen, Y. Zhu, and Y. Gao, "Rotatable antenna enabled spectrum sharing: Joint antenna orientation and beamforming design," arXiv preprint: 2509.19912, <https://arxiv.org/abs/2509.19912>, 2025.

[42] K. Pan *et al.*, "Rotatable antenna-enhanced cell-free communication," arXiv preprint: 2512.04742, <https://arxiv.org/abs/2512.04742>, 2025.

[43] C. A. Balanis, *Antenna theory: Analysis and design*. John Wiley & Sons, 2016.

[44] S. Boyd and L. Vandenberghe, *Convex Optimization*. Cambridge, U.K.: Cambridge Univ. Press, 2004.